A High-Precision Method for the Determination of Cavity Length of a Fabry-Perot Interferometer

Yunqing Guan, Biao Yin, and Xiaopeng Dong

***Abstract*—A novel method to obtain the cavity length of a Fabry-Perot interferometer (FPI) precisely based on the Vernier effect via a virtually variable reference FPI is proposed in this paper. Compared with the traditional method based on the measurement of wavelength spacing between two adjacent peaks in the spectrum of a single FPI, or enlarge the wavelength spacing with the Vernier effect by incorporating a real reference FPI in the sensor part, the present scheme is more flexible and applicable. By scanning the cavity length of the virtual reference FPI digitally, the accurate cavity length of the real FPI can be obtained when the free spectrum range (FSR) of the spectrum envelope of the combined FPIs reaches a maximum. Both theoretical analysis and experimental results show that the proposed scheme is superior to traditional methods, and with the present measurement condition, more than 20 times accuracy improvement for the determination of cavity length can be achieved.**

***Index Terms*—Cavity length, virtually variable reference FPI, Vernier effect.**

I. Introduction

As a type of optical interferometer, FPI has gained considerable attention and has been widely applied in various sensing purposes, such as refractive index [1], [2], temperature [3], [4], strain [5], [6], pressure [7], [8] and curvature [9]–[11], etc. For fiber-optic sensors based on FPIs, the signal demodulation methods can be divided to two types: the wavelength tracking method [12] and the peak-to-peak method [13], [14]. In comparison with the former method of tracking the peak or dip wavelength shift, which is hard to implement if a long term measurement is carried out and the power is incidentally off, or there are many similar periods in the spectrum, the measurement of cavity length of the FPI by the peak-to-peak method is superior since it will change monotonically with measurands. Therefore, measuring the cavity length of FPI with high precision is most important in practical applications.

Generally, the cavity length of an FPI, L, can be obtained from the FSR, which is defined by the wavelength difference between the two adjacent peak or dip wavelengths, λ_1 and λ_2, of the transmission or reflection spectrum of the FPI [14], [15]:

$$L = \frac{\lambda_1 \lambda_2}{2nFSR} \tag{1}$$

where n is the refractive index of the cavity medium. The accuracy of the cavity length obtained from Eq. (1) is then highly dependent on the measurement accuracy of the two wavelengths, λ_1 and λ_2, respectively. Consequently, the error of cavity length calculated from Eq. (1) can be expressed as:

$$\Delta L = \left| \frac{\lambda_1 \lambda_2}{2n\left(\lambda_2 - \lambda_1\right)} - \frac{\left(\lambda_1 - \Delta\lambda_1\right)\left(\lambda_2 - \Delta\lambda_2\right)}{2n\left(\lambda_2 - \lambda_1 - \Delta\lambda_2 + \Delta\lambda_1\right)} \right| \tag{2}$$

where $\Delta\lambda_1$ and $\Delta\lambda_2$ are the measurement errors of λ_1 and λ_2, respectively. If we suppose the wavelength measurement errors are the same for λ_1 and λ_2, i.e., $\Delta\lambda_1 = \Delta\lambda_2 = \Delta\lambda$, Eq. (2) can be simplified as follows:

$$\Delta L = \left| \frac{\lambda_1 \lambda_2 - \left(\lambda_1 - \Delta\lambda\right)\left(\lambda_2 - \Delta\lambda\right)}{2n\left(\lambda_2 - \lambda_1\right)} \right| \tag{3}$$

The measurement accuracy of the cavity length cannot be improved simply by using two wavelengths spaced across a number of spectral periods, since the FSR is not a constant at the measurement range of wavelength. It is well known the sensitivity of an interferometric sensor such as FPI can be increased by introducing a reference FPI in the measurement arrangement with its FSR closing to the sensing FPI, so, based on the Vernier effect, the wavelength shift or change of FSR can be effectively enlarged in the combined spectrum [16]–[19]. Therefore, if a reference FPI with variable FSR can be added to the measurement system, it is possible to increase the measurement accuracy of cavity length of sensing FPI greatly. However, in practice, a reference FPI with accurate FSR can hardly be built, and it is difficult to make the reference FPI immune to surrounding disturbance. Therefore, to get rid of the problem, we propose a novel method for the first time in this paper, that by introducing a virtual reference FPI with variable FSR, i.e., adjusting digitally the cavity length of a virtual FPI to match the cavity length of the sensing FPI. Owing to the Vernier effect, the FSR of the envelope of the superimposed spectrum, FSR_E, will increase dramatically up to infinity when the cavity length of the virtual reference FPI approaches that of the sensing FPI. So, by scanning the cavity length of the virtual reference FPI digitally, which is able to be carried out at most precision, with the aid of the Vernier effect, the cavity length of sensing FPI can be obtained with extremely high accuracy. The theoretical analysis and experimental measurement presented in

Manuscript received January 23, 2022; revised March 9, 2022; accepted March 24, 2022. Date of publication April 5, 2022; date of current version April 28, 2022. This work was supported in part by the National Natural Science Foundation of China under Grant 61775186, in part by the project from the Fundamental Bureau of Water Resources and Hydropower of China, and in part by the Marine and Fisheries Bureau of Xiamen under Grant 16CZB025SF03. *(Corresponding author: Xiaopeng Dong.)*

The authors are with the School of Electronic Science and Engineering, Institute of Lightwave Technology, Xiamen University, Xiamen 361005, China (e-mail: yunqingguan@stu.xmu.edu.cn; yinbiao@stu.xmu.edu.cn; xpd@xmu.edu.cn).

Digital Object Identifier 10.1109/JPHOT.2022.3163282

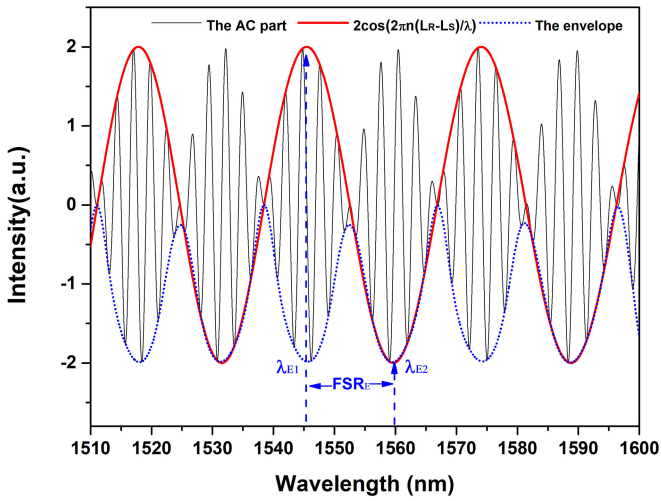

Fig. 1. Simulated AC part I'_{ac} of the total output according to Eq. (7) (L_R = 380 um, L_S = 465 um, $n = 1$).

the following sections demonstrate the validity of the proposed method.

II. Theoretical Analysis

The theoretical model for the combination of a sensing FPI and a virtual reference FPI, which is supposed in our analysis, can be analogized as two FPIs connected in parallel [16]. If the waves from different FPIs are incoherent, the total output of the FPI combination can be written as:

$$I = I_R + I_S = 4I_0 + 2I_0 cos\phi_R + 2I_0 cos\phi_S \tag{4}$$

where I_R and I_S represent the optical intensity of the output from the virtual and sensing FPI, respectively. To simplify the expression, we assume that all the amplitudes of the reflected waves inside each FPI are the same, which is represented by I_0. ϕ_R and ϕ_S are the phase of the virtual and sensing FPI, which can be expressed as $\frac{4\pi nL_R}{\lambda}$ and $\frac{4\pi nL_S}{\lambda}$, where L_R and L_S are the cavity lengths of virtual and sensing FPI, respectively. Eq. (4) can be further divided into DC part I_{dc} and AC part I_{ac} by signal filtering, and I_{ac} can be further expressed as follows:

$$I_{dc} = 4I_0 \tag{5}$$

$$I_{ac} = 2I_0 \left(cos\frac{4\pi nL_R}{\lambda} + cos\frac{4\pi nL_S}{\lambda} \right) \tag{6}$$

$$I'_{ac} = 2cos\frac{2\pi n\left(L_R + L_S\right)}{\lambda} cos\frac{2\pi n\left(L_R - L_S\right)}{\lambda} \tag{7}$$

An example of the curve of I'_{ac} vs. λ is illustrated in Fig. 1. From Fig. 1, the envelope of the superimposed spectrum is obtained by fitting the valleys of the high-frequency fringes, for example, the lower envelope is shown by the blue line. It is clear that owing to the Vernier effect induced variation of the envelope of the superimposed spectrum, we can define a new FSR_E from the adjacent peak or dip wavelengths of the envelope, which is the wavelength difference between λ_{E1} and λ_{E2}. The phases at λ_{E1} and λ_{E2} can be expressed as $\frac{2\pi n(L_R - L_S)}{\lambda_{E1}}$ and $\frac{2\pi n(L_R - L_S)}{\lambda_{E2}}$, respectively, the difference between them is shown by the blue arrows in Fig. 1, which can be expressed as:

$$\left| \frac{2\pi n\left(L_R - L_S\right)}{\lambda_{E1}} - \frac{2\pi n\left(L_R - L_S\right)}{\lambda_{E2}} \right| = \pi \tag{8}$$

Then, FSR_E, which is defined by the wavelength difference between the two adjacent peak or dip wavelengths of the envelope, λ_{E1} and λ_{E2}, can be derived from Eq. (8) and the relation between FSR_E and the FSRs of reference FPI and sensing FPI can be expressed as [20], [21]:

$$\begin{aligned} FSR_E &= |\lambda_{E2} - \lambda_{E1}| = \frac{\lambda_{E1}\lambda_{E2}}{|2n\left(L_R - L_S\right)|} \\ &= \frac{FSR_R * FSR_S}{|FSR_S - FSR_R|} \end{aligned} \tag{9}$$

Therefore, the cavity length L_S can be derived from Eq. (9) and its determination error $\Delta L'$ can be expressed as:

$$L_S = L_R \pm \frac{\lambda_{E1}\lambda_{E2}}{2nFSR_E} \tag{10}$$

$$\Delta L' = \left| \frac{\lambda_{E1}\lambda_{E2}}{2n\left(\lambda_{E2} - \lambda_{E1}\right)} - \frac{\left(\lambda_{E1} - \Delta\lambda_{E1}\right)\left(\lambda_{E2} - \Delta\lambda_{E2}\right)}{2n\left(\lambda_{E2} - \lambda_{E1} - \Delta\lambda_{E2} + \Delta\lambda_{E1}\right)} \right| \tag{11}$$

where $\Delta\lambda_{E1}$ and $\Delta\lambda_{E2}$ denote the measurement errors of λ_{E1} and λ_{E2}. Since the reference FPI superimposed on the sensing FPI is digitally constructed without measurement error, $\Delta\lambda_{E1}$ and $\Delta\lambda_{E2}$ are considered equal to the wavelength measurement error $\Delta\lambda$ in Eq. (3), so $\Delta L'$ is:

$$\Delta L' = \left| \frac{\lambda_{E1}\lambda_{E2} - \left(\lambda_{E1} - \Delta\lambda\right)\left(\lambda_{E2} - \Delta\lambda\right)}{2n\left(\lambda_{E2} - \lambda_{E1}\right)} \right| \tag{12}$$

To compare the error of the cavity length calculated by the proposed method with that of the conventional method, an improvement factor m is introduced in the following analysis. The parameter m is similar to the amplification factor *M* in [16]. m can be obtained from Eq. (3) and Eq. (12) as follows:

$$m = \frac{\Delta L}{\Delta L'} = \frac{\Delta\lambda^2 - \left(\lambda_{E1} + \lambda_{E2}\right)\Delta\lambda}{\Delta\lambda^2 - \left(\lambda_1 + \lambda_2\right)\Delta\lambda} \frac{FSR_E}{FSR_S} \tag{13}$$

The value of $\lambda_{E1} + \lambda_{E2}$ and $\lambda_1 + \lambda_2$ can be considered to be approximately equal in Eq. (13) since both of them have the same center wavelength, consequently, Eq. (13) can be further simplified as:

$$m = \frac{FSR_E}{FSR_S} = \frac{FSR_R}{|FSR_S - FSR_R|} = \frac{1}{\left|\frac{L_R}{L_S} - 1\right|} \tag{14}$$

Then, we can get the relation between m and $\frac{L_R}{L_S}$ according to Eq. (14), as shown in Fig. 2. From Fig. 2, it can be seen that the closer L_R and L_S are, the greater value of m is. Meanwhile, according to Eq. (9), FSR_E becomes larger as well, but at least one complete FSR_E must be included in the wavelength range of the superimposed spectrum, which means the wavelength range of the spectrometer limits the value of m directly.

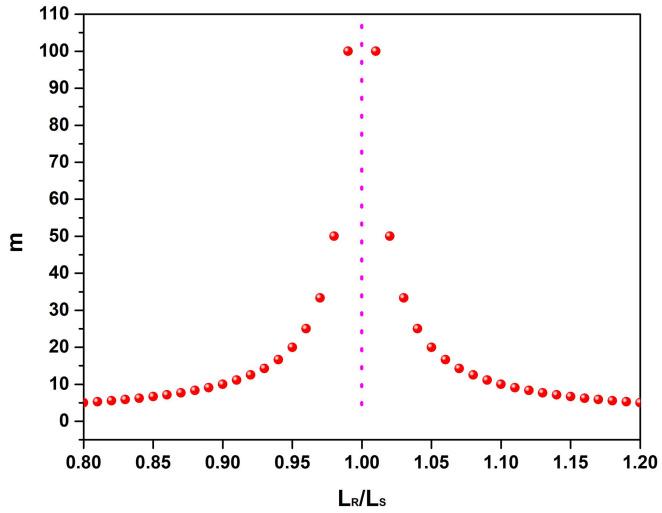

Fig. 2. The curve of m vs. $\frac{L_R}{L_S}$.

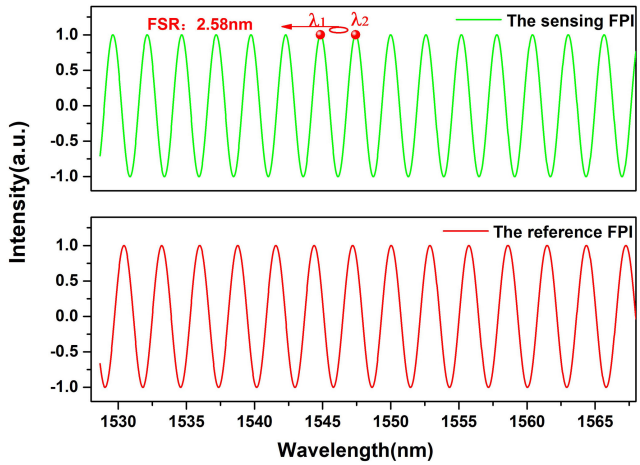

Fig. 3. The spectrums of the sensing FPI and reference FPI in simulation (L_S = 465 um, L_R = 423.16 um, n = 1).

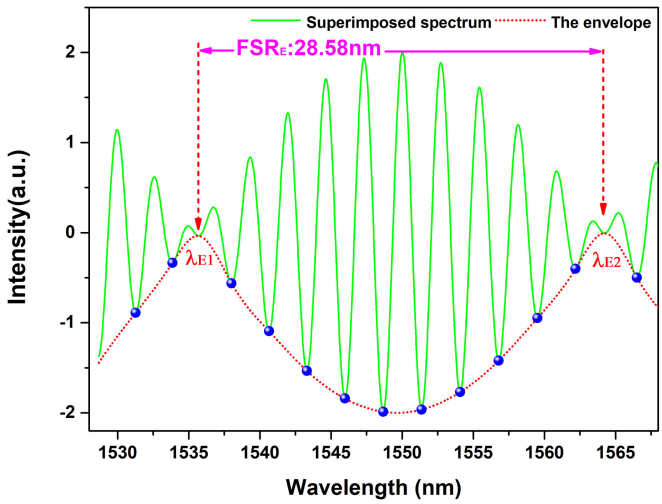

Fig. 4. The superimposed spectrum when the reference cavity length is 423.16 um in simulation.

The relation between the accuracy improvement factor m and the wavelength measurement range of the spectrometer should be studied. In theory, from Eq. (14) in the original submitted version, for the same sensing FPI, that is, when L_S and FSR_S remain unchanged, m and FSR_E is positively correlated. Then, according to Eq. (9), when the difference between the cavity length of the reference cavity and the cavity length of the sensing cavity becomes smaller, FSR_E becomes larger. Since we can flexibly construct a digital reference cavity with any cavity length, the maximum FSR_E as well as m can be obtained when the difference of the cavity length is minimum. However, in practical applications, FSR_E must be less than or equal to the measuring range of the spectrometer. So, FSR_E and m will increase when the measurement range of the spectrometer expands, which also explains that 12 times higher accuracy with 50 nm and 20 times higher with 100 nm range.

The numerical simulation is used to verify the applicability and flexibility of this method, we set the sensing FPI cavity length as 465 um, and the wavelength range of the spectrum is 1528 nm to 1568 nm as an example. The spectrum of the sensing FPI can be constructed, which is shown in Fig. 3, according to the following equation.

$$I_S = cos\frac{4\pi n L_s}{\lambda} \tag{15}$$

In the traditional method, the two adjacent peaks around 1545 nm are substituted into Eq. (1), which are shown by the red dots in Fig. 3. It can be calculated that the cavity length is 462.96 um and the error ΔL is 2.04 um.

Here, the proposed method is used to improve the accuracy of the cavity length. First, the cavity length of the virtual reference cavity needs to be determined. Considering the sensing cavity length obtained by the traditional method is 462.96 um and the wavelength range of the spectrum is 40 nm, which must include at least one complete FSR_E. We set $\lambda_{E1}\lambda_{E2}$ as 1545 nm $*$ 1545 nm, L_S as 462.96 um, and FSR_E as 30 nm. 30 nm is an example to ensure that a full period of the envelope is included in the measurement range of the spectrometer, the reference cavity length L_R is calculated as 423.16 um according to Eq. (9). The virtual reference FPI spectrum can be constructed with L_R instead of L_S according to Eq. (15). Then, the obtained virtual reference FPI spectrum is superimposed with the sensing FPI spectrum, the superimposed spectrum is formed in the shape of the large envelope, thus, 1535.63 nm and 1564.21 nm are λ_{E1} and λ_{E2} as the arrows shown in Fig. 4. The envelope FSR_E is 28.58 nm, so the sensing cavity length L_S is calculated as 465.18 um according to Eq. (10). The corresponding error $\Delta L'$ is 0.18 um and the improvement factor m is 11.52 according to Eq. (13).

Moreover, to verify the relation between m and $\frac{L_R}{L_S}$, variable virtual reference cavity lengths are substituted into Eq. (10) to calculate sensing cavity length. The result is shown in Table I.

It can be seen from the table that when the selected reference cavity length makes $\frac{L_R}{L_S}$ closer to 1, the improvement factor m becomes higher, which is consistent with Fig. 2.

TABLE I
THE RELATION BETWEEN m AND $\frac{L_R}{L_S}$

L_R (um)	$\frac{L_R}{L_S}$	L_S calculated by Eq. (10) (um)	Error percentage (%)	m calculated by Eq. (13)
423.16	0.92	465.18	0.039	11.52
410	0.89	465.31	0.067	6.58
400	0.86	465.67	0.14	3.30
390	0.84	466.06	0.23	1.91

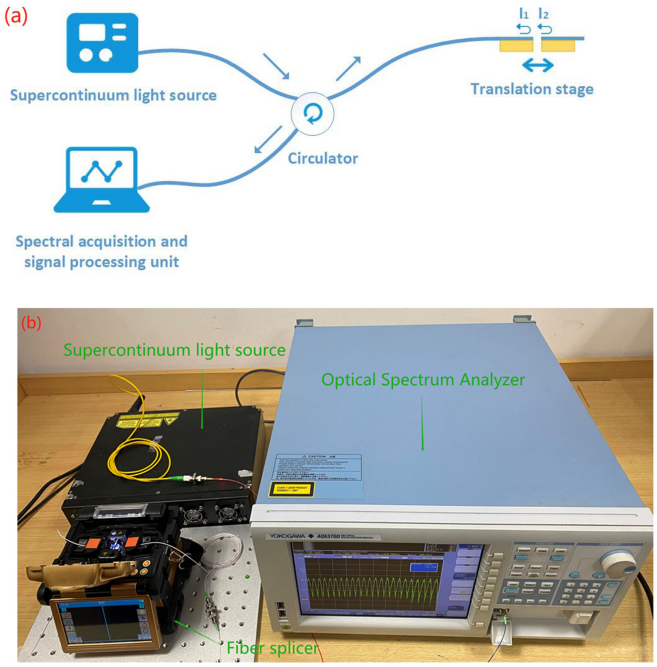

Fig. 5. (a) Schematic diagram of the experimental setup for displacement measurement. (b) The real photo of the experimental setup.

III. EXPERIMENTAL EXAMPLE OF A DISPLACEMENT MEASUREMENT

To verify the validity of the accurate determination method of the cavity length of an FPI, a displacement measurement setup is established, and the experimental arrangement is illustrated in Fig. 5(a) and Fig. 5(b). A broadband supercontinuum light source (BBS) with a wavelength range from 800 nm to 2100 nm is employed in the measurement. The light outputting from the BBS will propagate to the optical circulator, which will direct it to the FPI under test (FPI-UT). The FPI is comprised of a single-mode fiber with a well cleaved end and another aligned fiber with a gap between them. The separation of the two ends of the aligned fibers forms the cavity of the FPI. Without loss of generality, a fiber splicer is employed to adjust the separation of the ends, so, the fibers are mounted onto the translation stages of the splicer. Consequently, the cavity length of FPI can be changed manually.

To get the exact cavity length as calibration, an image processing method is used to extract the number of pixels corresponding to the fiber diameter. A known cladding diameter of 125 um corresponds to 992 pixels with an error of 1 pixel is shown in Fig. 6(a) and Fig. 6(b). The number of pixels corresponding to

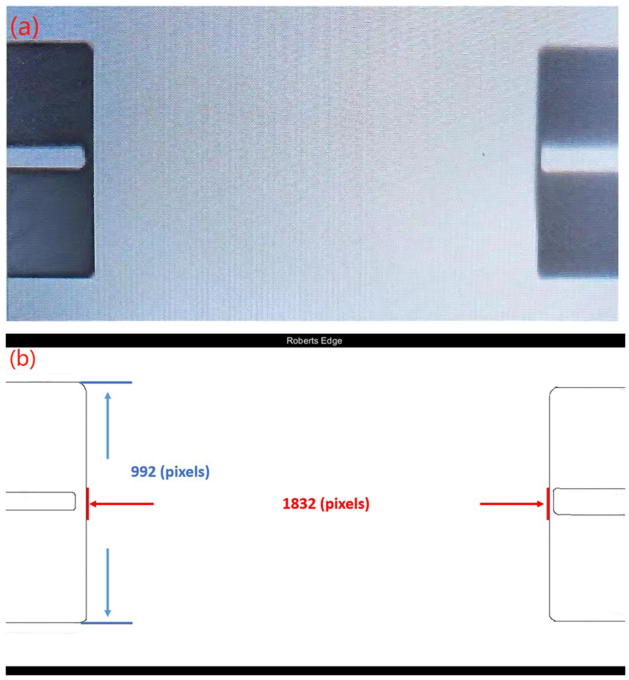

Fig. 6. (a) The original picture of FP cavity displayed by the fiber splicer. (b) The original picture after image edge extraction.

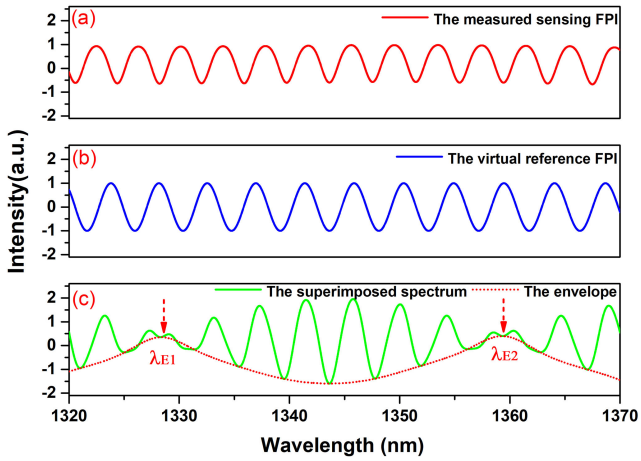

Fig. 7. The spectrums in the experiment when the measurement range of the OSA is 50 nm. (a) The spectrum of sensing FPI. (b) The spectrum of reference FPI. (c) The superimposed spectrum.

the cavity length is 1832, so the cavity length is 230.85 um with an error of 0.126 um. The image method is also used in [22].

The reflected spectrum of the FPI can be measured by the Optical Spectrum Analyzer (Yokogawa, AQ6370D). Take the measurement range of 50 nm as an example, the two adjacent peaks around 1345 nm are substituted into Eq. (1) as λ_1 and λ_2 by the conventional method. The cavity length of FPI-UT can be obtained as 233.42 um from the measurement result of FSR calculated from its spectrum, which is given in Fig. 7(a). The error percentage of the conventional method is 1.11% according to the accurate value of cavity length obtained by the image method (230.85 um) as the calibration.

TABLE II
THE COMPARISON OF THE KEY PARAMETERS BETWEEN THE PROPOSED METHOD AND OTHERS

	Whether can get absolute cavity length	Measurement Range	Error percentage (%)	Cavity length accuracy
Wavelength tracking method in [12]	No	Limited to FSR	NA	NA
Peak-to-peak method in [13]	Yes	Limited to the range of the spectrometer	16.67%	Low
Peak-to-peak method in [14]	Yes	Limited to the range of the spectrometer	0.59%	Medium
This method	Yes	Limited to the range of the spectrometer	0.09%	High

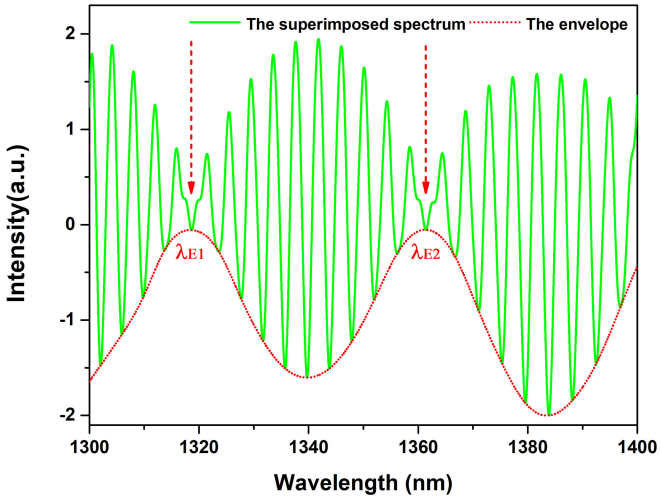

Fig. 8. The superimposed spectrum in the experiment when the measurement range of the OSA is 100 nm.

In the proposed method, the cavity length of the virtual reference FPI needs to be determined. To ensure that at least one complete FSR_E is included in the measurement range of the OSA (50 nm) which is mentioned in the previous section. FSR_E can be chosen as 30 nm as an example, the two adjacent peaks around 1345 nm as λ_{E1} and λ_{E2} and L_S as 233.42 um are substituted into Eq. (9). Then the cavity length of the virtual reference FPI is calculated as 202 um. The spectrum of the virtual FPI is shown in Fig. 7(b) according to Eq. (15) with L_R instead of f L_S. Then, the superimposed spectrum can be obtained, which is shown in Fig. 7(c). Finally, the accurate values of λ_{E1} and λ_{E2} can be obtained from the superimposed spectrum as shown in Fig. 7(c). According to Eq. (9), the result of sensing FPI cavity length is calculated as 231.05 um. The error percentage of the proposed method is 0.09%. Compared with the conventional method, 12 times higher accuracy has been achieved, which is consistent with the simulation. We changed the displacement that is the cavity length of the sensing FPI to verify the repeatability and reproducibility of the proposed method. When the cavity lengths are 219.67 um, 221.61 um, and 235.20 um in order, the values of m that can be calculated according to Eq. (13) are 11, 12, and 12 in sequence. Moreover, the comparison of the key parameters between the proposed method and the ones in the literature is shown in Table II for a clearer comparison.

To get higher precision, we adjusted the measurement range of the OSA to 100 nm. The superimposed spectrum can be obtained by the proposed method and the envelope can be extracted, which are shown in Fig. 8. Through the proposed method, the result of sensing FPI cavity length is calculated as 230.98 um. The error percentage of the proposed method is 0.05%. Compared with the conventional method, at least 20 times higher accuracy can be achieved at present measurement parameters, such as the wavelength range is 100 nm. The accuracy can be further increased if a larger wavelength range is selected in the measurement.

IV. CONCLUSION

The novel method for the determination of the cavity length of an FPI based on the Vernier effect through a virtually variable reference FPI has been demonstrated. The theoretical analysis and experimental results show the measurement accuracy can be effectively improved by measuring the transmission or reflection spectrum of the FPI in a large wavelength range and constructing a composited spectrum with the Vernier effect by digitally scanning the cavity length of a virtual reference FPI. The novel method provides a new approach to obtain the cavity length of an FPI, or more generally the optical path difference (OPD) of an interferometer with high accuracy, and without the cost of building a real reference FPI and the stability problem met in the experiment.

REFERENCES

[1] T. Wei, Y. Han, Y. Li, H.-L. Tsai, and H. Xiao, "Temperature-insensitive miniaturized fiber inline Fabry-Perot interferometer for highly sensitive refractive index measurement," *Opt. Exp.,* vol. 16, no. 8, pp. 5764–5769, Apr. 14, 2008.

[2] P. Chen, X. Shu, and H. Cao, "Novel compact and low-cost ultraweak Fabry-Perot interferometer as a highly sensitive refractive index sensor," *IEEE Photon. J.,* vol. 9, no. 5, Oct. 2017, Art. no. 7105810.

[3] X. Q. Lei and X. P. Dong, "High-sensitivity Fabry-Perot interferometer high-temperature fiber sensor based on vernier effect," *IEEE Sens. J.,* vol. 20, no. 10, pp. 5292–5297, May 2020.

[4] K. Yang *et al.*, "Ultrasensitive temperature sensor based on a fiber Fabry-Perot interferometer created in a mercury-filled silica tube," *IEEE Photon. J.,* vol. 7, no. 6, Dec. 2015, Art. no. 6803509.

[5] S. Liu *et al.*, "High-sensitivity strain sensor based on in-fiber improved Fabry-Perot interferometer," *Opt. Lett.,* vol. 39, no. 7, pp. 2121–2124, Apr. 2014.

[6] L. Liu *et al.*, "High-sensitivity strain sensor implemented by hybrid cascaded interferometers and the Vernier-effect," *Opt. Laser Technol.,* vol. 119, Nov. 1, 2019, Art. no. 105591.

[7] N. Dong, S. Wang, L. Jiang, Y. Jiang, P. Wang, and L. Zhang, "Pressure and temperature sensor based on graphene diaphragm and fiber Bragg gratings," *IEEE Photon. Technol. Lett.,* vol. 30, no. 5, pp. 431–434, Mar. 2018.

[8] S. Ghildiyal, P. Ranjan, S. Mishra, R. Balasubramaniam, and J. John, "Fabry-Perot interferometer-based absolute pressure sensor with stainless steel diaphragm," *IEEE Sens. J.,* vol. 19, no. 15, pp. 6093–6101, Aug. 2019.

[9] A. G. Leal, L. M. Avellar, C. A. R. Diaz, A. Frizera, C. Marques, and M. J. Pontes, "Fabry-Perot curvature sensor with cavities based on UV-curable resins: Design, analysis, and data integration approach," *IEEE Sens. J.,* vol. 19, no. 21, pp. 9798–9805, Nov. 2019.

[10] F. X. Zhu *et al.*, "Fabry-Perot vector curvature sensor based on cavity length demodulation," *Opt. Fiber Technol.*, vol. 60, Dec. 2020, Art. no. 102382.

[11] Y. Guo and Y. D. Zhang, "A new bamboo-shaped sensor for curvature measurement with microstructured fiber," *IEEE Photon. Technol. Lett.,* vol. 33, no. 12, pp. 619–622, Jun. 2021.
[12] G. G. Liu, W. L. Hou, and M. Han, "Unambiguous peak recognition for a silicon Fabry-Perot interferometric temperature sensor," *J. Lightw. Technol.*, vol. 36, no. 10, pp. 1970–1978, May 2018.
[13] S. Watson *et al.*, "Laser-machined fibers as Fabry-Perot pressure sensors," *Appl. Opt.*, vol. 45, no. 22, pp. 5590–5596, Aug. 2006.
[14] Y. Jiang, "High-resolution interrogation method for fiber optic extrinsic Fabry-Perot interferometric sensors by the peak-to-peak method," *Appl. Opt.,* vol. 47, no. 7, pp. 925–932, Mar. 2008.
[15] J.-R. Zhao, X.-G. Huang, W.-X. He, and J.-H. Chen, "High-resolution and temperature-insensitive fiber optic refractive index sensor based on fresnel reflection modulated by Fabry-Perot interference," *J. Lightw. Technol.,* vol. 28, no. 19, pp. 2799–2803, Oct. 2010.
[16] D. Dai, "Highly sensitive digital optical sensor based on cascaded high-Q ring-resonators," *Opt. Exp.,* vol. 17, no. 26, pp. 23817–23822, Dec. 2009.
[17] T. Yao, S. Pu, Y. Zhao, and Y. Li, "Ultrasensitive refractive index sensor based on parallel-connected dual Fabry-Perot interferometers with Vernier effect," *Sens. Actuator A Phys.,* vol. 290, pp. 14–19, May 2019.
[18] L.-Y. Shao *et al.*, "Sensitivity-enhanced temperature sensor with cascaded fiber optic Sagnac interferometers based on Vernier-effect," *Opt. Commun.,* vol. 336, pp. 73–76, Feb. 2015.
[19] C. Lu, X. Dong, L. Lu, Y. Guan, and S. Ding, "Label free all-fiber static pressure sensor based on Vernier effect with temperature compensation," *IEEE Sens. J.,* vol. 20, no. 9, pp. 4726–4731, May 2020.
[20] Y. Wu *et al.*, "A transverse load sensor with ultra-sensitivity employing Vernier-effect improved parallel-structured fiber-optic Fabry-Perot interferometer," *IEEE Access,* vol. 7, pp. 120297–120303, 2019.
[21] H. Lin, F. Liu, H. Guo, A. Zhou, and Y. Dai, "Ultra-highly sensitive gas pressure sensor based on dual side-hole fiber interferometers with Vernier effect," *Opt. Exp.,* vol. 26, no. 22, pp. 28763–28772, Oct. 2018.
[22] L. H. Chen *et al.*, "Chitosan based fiber-optic Fabry-Perot humidity sensor," *Sens. Actuators B Chem.*, vol. 169, pp. 167–172, Jul. 2012.